

High signal-to-noise detection of rotational Raman scattering through refluorescent and dispersive atomic filters

Richard B. Miles,^{1*} Zhen Tang,¹ Sohail H. Zaidi,¹ Azer Yalin¹ and Noah Finkelstein²

¹ Department of Mechanical and Aerospace Engineering, Princeton University, Olden Street, Princeton, New Jersey 08544, USA

² University of California at San Diego, 9500 Gilman Drive, La Jolla, California 92093-0092, USA

We introduce new methods for capturing rotational Raman scattering that simultaneously suppress background scattering and have exceedingly high spectral dispersion at low wavenumbers. These methods are based on resonant absorption and refractive index dispersion of atomic vapor, and take advantage of the availability of tunable lasers. Three different configurations are presented. The first is an atomic notch transmission filter which is based on refluorescence from an optically thick atomic vapor cell. This configuration is demonstrated in air using mercury vapor at 254 nm. The second configuration is an atomic resonance prism cell which is demonstrated in CO₂ using mercury vapor, again at 254 nm. The third configuration is a density gradient atomic vapor cell which uses rubidium vapor at 780 nm. In the last two configurations, the atomic cell simultaneously blocks the elastic scattering while spatially dispersing the rotational Raman lines. In each case, a tunable Ti:sapphire laser was employed as an illuminating source. Copyright © 2000 John Wiley & Sons, Ltd.

INTRODUCTION

Raman scattering is an important tool for gas-phase diagnostics, since it allows one to measure species concentrations and also rotational and vibrational temperatures through the association of line strengths with population fractions. However, many applications of Raman scattering have been limited by both the low scattering cross-section and the presence of strong background scattering. These limitations have kept Raman scattering from becoming a practical tool for combustion or flow field diagnostics. Only through heroic experiments have multi-dimensional data been recorded.^{1–4}

In virtually all cases, the Raman spectrum that has been recorded is the vibrational Raman spectrum, corresponding to transitions between the ground vibrational state and the first excited vibrational state. It is important to recognize that, for most molecules, the rotational Raman cross-section is one to two orders of magnitude larger than the vibrational cross-section. The rotational Raman spectrum is not typically used for diagnostics because the rotational lines of the various species are interspersed with each other. Furthermore, the rotational Raman spectrum is very close to the Rayleigh line and other background scattering that often obscures it.

The availability of narrow linewidth lasers that can be tuned in the vicinity of atomic resonances offers a new approach to Raman spectroscopy. In this case, atomic filters can be used to provide very strong suppression of

background light while simultaneously providing spectral dispersion with high throughput. Three approaches are outlined in this paper. The first involves using refluorescence from an optically thick atomic mercury vapor cell.⁵ The second and third approaches rely on the dispersion of the atomic vapor near resonance. The second approach achieves this with an atomic mercury vapor prism,⁶ and the third with an atomic rubidium vapor density gradient cell (Z. Tang, S. H. Zaidi and R. B. Miles, Paper AIAA-2000-0644 presented at the 38th Aerospace Sciences Meeting and Exhibition January 10–13, 2000, Reno, NV). In the refluorescence case, the narrow linewidth of the atomic resonance, together with time gating, provides strong suppression of background light, and two-dimensional images can be taken. In the prism and density gradient cell cases, the resonant absorption of the atomic vapor provides the background suppression, and the refractive index variation of the atomic vapor disperses the Raman spectrum. In these cases, one-dimensional images are achievable.

MERCURY VAPOR REFLUORESCENCE FILTER

Recent work has established the utility of an optically thick, atomic blocking, notch filter for the acquisition of Rayleigh scattering data in air.⁷ The filter serves two major functions. By tuning the laser to the center of the filter resonance, the filter serves to suppress strongly elastic background scattering that often arises from particles and from the windows and walls of the experimental chamber. The second function is to permit the spectrum of the Rayleigh scattering to be resolved by tuning the laser frequency relative to the atomic resonance and recording the scattering transmitted through the cell as a function of that

* Correspondence to: R. B. Miles, Department of Mechanical and Aerospace Engineering, Princeton University, Olden Street, Princeton, New Jersey 08544, USA; e-mail: miles@princeton.edu
Contract/grant sponsor: Air Force Office of Scientific Research.
Contract/grant sponsor: M. L. Energia, Inc.

laser frequency. By deconvolving the spectral shape of the atomic transmission from the recorded transmission signal, the spectrum of the Rayleigh scattering is retrieved.⁸

Extending this approach to Raman scattering requires that the strong Rayleigh scattering be suppressed at all times, since that can be more than three orders of magnitude greater than the Raman signal. Since the Rayleigh signal is offset in frequency from the Raman signal, a notch passband rather than a notch blocking filter is required. If such a filter can be designed, then the laser is tuned so the frequency of the Raman light overlaps the passband, and all other scattering is blocked. It is also important to maintain an imaging capability through such a filter and to have a large acceptance angle for good field-of-view and efficient light collection. Background suppression needs to be great enough to allow the Raman scattering to be uncontaminated by other light scattering, whether that be Rayleigh, particle, fluorescence or background from windows and walls.

The two approaches that have been previously proposed for this type of notch passband filter are a double resonance atomic fluorescence cell and atomic Faraday and Voigt filters. The double resonance cell is a device that uses either a local laser,^{9,10} or collisions with a rare gas¹¹ to transfer atoms from a state which has been driven by the incident light to a second state which fluoresces at a different wavelength. Fluorescence is then collected by a sensitive detector. Since the fluorescence is at a very different frequency than either the local laser or the scattered light, standard Schott glass or interference filters can be used to reject the incident and local laser light and pass the fluorescence. Generally, this device has no imaging capability and there may be significant light loss in the system through the 4π refluorescence solid angle and the transfer efficiency of the laser or rare gas collision process.

The Faraday and Voigt filters rely on the polarization rotation that occurs in an atomic vapor near resonance in the presence of a magnetic field.¹² This leads to optical rotation of light propagating through the cell. If polarizers are placed at the entrance and at the exit of the cell, then off-resonance light will not pass, but light which falls close to the atomic resonance can pass through. The Faraday and Voigt approaches have good throughput, but the background rejection is very sensitive to the optical quality of the polarizers and the light propagation angle. Rejection of on axis light is rarely better than two orders of magnitude. The small acceptance angle precludes imaging applications, and the rejection is probably too small to permit Raman spectroscopy.

These limitations are overcome by using an optically thick atomic vapor refluorescence cell as a narrow band, notch transmission filter.⁵ If the atomic transition is to the ground state and there are no other allowed transitions down from the upper state, then light which is absorbed by that transition is re-radiated at the same frequency. This leads to the well-known phenomenon of optical trapping. In an optically thick cell, the on-resonance light entering the cell is absorbed within the first few tens of microns. When this light is re-radiated, the light emitted back toward the entrance window exits the cell, whereas the light which is re-radiated toward the interior of the cell is immediately reabsorbed. When that light is again re-radiated, the portion which is re-radiated back toward the entrance window escapes, and the portion headed farther into the cell is again absorbed. Through

this iterative process, in the absence of quenching, all the light is finally re-radiated back out of the entrance window, with an effective radiation lifetime several times longer than the isolated atom radiation lifetime. If the cell has sufficient optical thickness, this whole process remains very well localized, so the re-radiated light exits the cell at approximately the same location it entered. Light which is not at the atomic resonance frequency passes through the cell. Hence this type of cell can serve as a notch transmission filter by detecting only the re-radiated light. This re-radiated light can be collected through a narrow linewidth interference filter, if necessary, for further background rejection. Even greater rejection of out-of-band light can be achieved by using a pulsed laser to generate the Raman scattering, time-gating the detector to be off during the laser pulse, and then immediately turned on so that only the refluorescence is seen. Any light reflected off the surface of the cell is then rejected since that light will only be present during the laser pulse. Since the absorption length is so small and the refluorescence remains localized, this cell can be used for imaging.¹³

Various factors must be weighed in the selection of an appropriate atomic vapor. The atomic vapor must have a strong, optically thick transition from the ground state and needs to overlap some available narrow linewidth, tunable laser frequency. In order to have good discrimination, the spectral profile of the optically thick filter should be as close to a notch as possible. The ideal notch filter would have no 'transmission' out of band, so the absorption of the atomic vapor in the optically thick regime should quickly go to zero. If the atomic vapor is naturally or collision broadened, then the lineshape of the absorption constant is Lorentzian and falls off from line center as $1/1 + (\delta\omega)^2$, where $\delta\omega$ is the frequency offset from line center normalized by the linewidth. If, on the other hand, the atomic vapor line is thermally broadened, then the lineshape is Gaussian and the absorption constant falls off as $e^{-(\delta\omega)^2}$. The exponential fall off leads to orders of magnitude less out of band absorption, particularly in the optically thick regime, so it is important to operate the atomic filter at low enough pressure that the lineshape is dominated by thermal broadening. The sharpness of the thermally broadened filter is determined by the ratio of the temperature to the mass, so the sharpest filters use an atomic vapor with a high atomic mass and high vapor pressure (low boiling point). The best candidates for atomic refluorescence filters are mercury, rubidium and cesium vapor. For Raman scattering, the scattering cross-section increases as the fourth power of the scattering frequency. The mercury transition is in the ultraviolet region where this enhancement is substantial, whereas cesium and rubidium are in the infrared region at frequencies where strong narrow linewidth solid-state and diode lasers are available, but where Raman scattering is weak. For the refluorescence experiments reported here, mercury vapor was used and illumination was provided by a tunable, injection locked, frequency-tripled Ti : sapphire laser.

Figure 1 shows a diagram of the setup. The frequency-tripled Ti : sapphire laser was focused into air. The Raman scattering was collected at 90° and imaged on to an optically thick mercury vapor cell. The light that was refluoresced was collected and imaged with a camera that views the front surface of that cell.

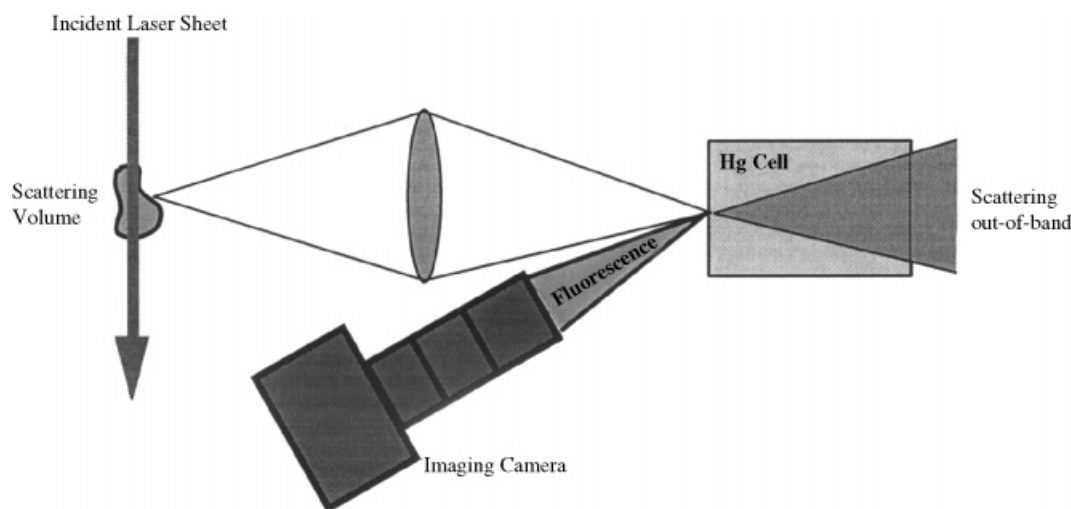


Figure 1. Narrow passband imaging filter layout. Scattering from an interrogation volume is imaged on to the inside surface of a mercury vapor cell. Light coincident with the ground-state transition at 253.7 nm is fluoresced and imaged by a camera.

Figure 2 shows the absorption and refluorescence spectra of the mercury vapor cell. The mercury side-arm was maintained at a temperature of approximately 25 °C, and the cell was heated to avoid mercury condensation on the windows. This temperature corresponds to a vapor pressure of 0.002 Torr (1 Torr = 133.3 Pa). The spectral features of the absorption bands are due to the various isotopic species and hyperfine states. Note that the absorption and refluorescence spectra are nearly the inverse of one another, demonstrating that the refluorescence cell can be operated as an effective bandpass filter.

Figure 3 shows the refluorescence signal collected as a function of time for a factor of 20 range of mercury vapor pressures. Note that there is very little change and that the refluorescence time is 450 ns, which is slightly less than four times the 120 ns natural lifetime of mercury vapor. For Fig. 2, the detector was gated 60 ns after the laser pulse and integrated the signal for 4 μ s. The spatial resolution of the cell is determined by the penetration depth of the resonant light, and improves at higher vapor pressures. At 0.05 Torr (70 °C side-arm temperature), the penetration depth at the mercury-202 line frequency is 35 μ m. Under these conditions a resolution of approximately 100 μ m

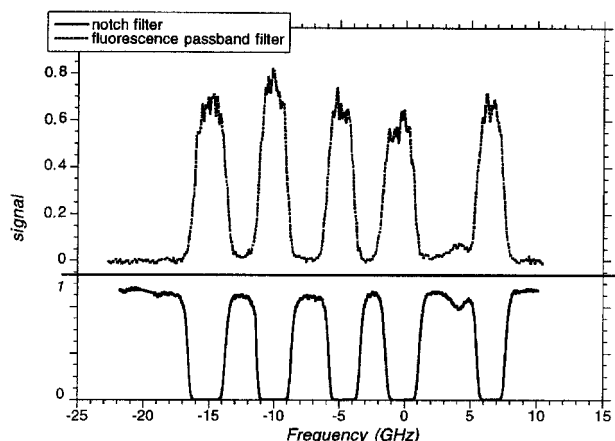


Figure 2. Narrow passband filter and notch absorption filter: spectral profiles. Simultaneous spectral scans of the Hg cell operating in two modes. Above, narrow passband; below, notch absorption. The bands arise from naturally occurring isotopes.

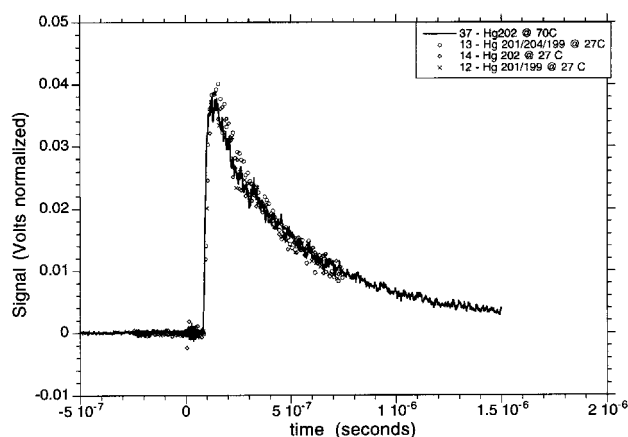


Figure 3. Narrow passband filter: temporal response for varying number density. Number density varies by a factor of 20 for Hg-202 and a factor of two between isotopes.

is achievable for short imaging delay times. At longer delays the resolution degrades due to photon and particle diffusion inside the cell.

As the laser is tuned, the rotational Raman lines from the air are sequentially scanned through the atomic mercury vapor resonance. The refluorescence from the entrance face of the cell is collected by a lens and directed on to a photomultiplier tube through a narrow line interference filter centered at 254 nm, the mercury vapor resonance frequency. Only the light that is close to the mercury resonance frequency passes through the filter. This rejects laser-induced fluorescence and other light that is far from the mercury resonance line. The signal from the photomultiplier tube is time gated to exclude the time interval when the Ti : sapphire laser is on, so Rayleigh and background scattering from the laser that might be reflected off the surface of the mercury cell is further rejected. With this configuration, a rotational Raman spectrum of the air can be taken with virtually no background noise.

Figure 4 shows a portion of the rotational Raman spectrum of both oxygen and nitrogen in the air taken with a mercury cell vapor pressure of 0.1 Torr (100 °C side-arm temperature). The laser pulse length is approximately 10 ns, and the linewidth is close to the transform limit.

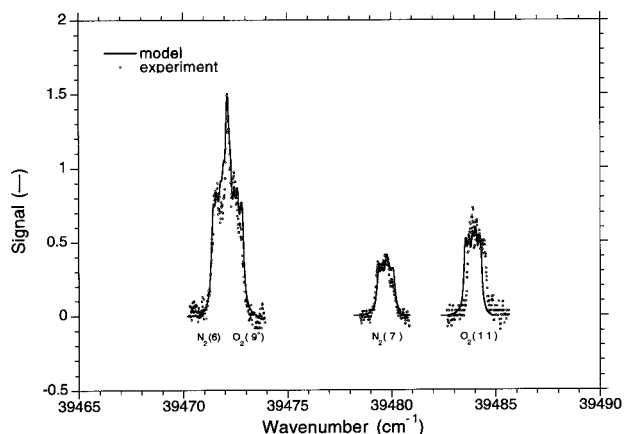


Figure 4. Rotational Raman scattering from room air. Experiment and model predictions. Model includes rotational Raman broadened lineshape convolved with Monte Carlo model for the passband filter. Three different spectral scans cover four individual rotational Raman lines.

The laser is frequency tripled to yield 10 mJ pulses tunable in the vicinity of 253.7 nm. The lines are identified in the figure, and the structure associated with each line represents the isotopic and hyperfine structure of the filter itself. It is interesting to note that the oxygen lines are stronger than the nitrogen lines, even though the mole fraction of oxygen is one quarter that of nitrogen. This occurs because the oxygen Raman polarizability is resonantly enhanced by the UV Schumann Runge band. The spectra in Fig. 4 were taken with three different laser scans and represent 30 shot averages. The refluorescence efficiency is estimated to be 80%, with the loss primarily due to quenching and optical trapping. In addition, some loss (6–8% per surface) occurs at the windows. The major inefficiency in this experiment occurs from the losses associated with the recollection of the fluorescent light re-radiated as Lambertian surface emission from the front of the cell. The collection efficiency, η , is

$$\eta = \frac{1}{4(f^\#)^2 \left[1 + \frac{1}{m} \right]^2 + 1}$$

where $f^\#$ is the f number of the collection lens ($f^\# = \text{focal length/lens diameter}$) and m is the magnification.

An $f/1$ lens only collects 20% of that light. In the experimental setup used for the data shown above, an $f/4.5$ lens was used with a magnification of 1.5, so only

0.44% of the refluorescent light was collected. For non-imaging applications, better efficiency can be achieved, for example, by using a compound parabolic concentrator simultaneously to focus on the cell and collect the refluorescence.¹⁴

ATOMIC MERCURY VAPOR PRISM

The second and third approaches to Raman imaging with an atomic filter take advantage of the resonant dispersion of the atomic vapor in the vicinity of the atomic transition. In these cases, the entire spectrum can be simultaneously observed, and the cell throughput is high. If desired, the scattering along a line can be imaged in the direction orthogonal to the spectral dispersion of the filter. The dispersion can be achieved either using a prism configuration or a density gradient. A mercury prism cell is discussed here, and a gradient rubidium dispersion cell is presented in the next section.

A diagram of the mercury vapor cell is shown in Fig. 5. The cell is configured like a prism, with the windows at Brewster's angle for the 253.7 nm resonance light. When the Raman light passes through the cell, the strong variation in the refractive index causes the light to be bent at the interface in accord with Snell's law. In this configuration, the dispersion of the mercury vapor can be measured by recording the displacement of the laser as a function of laser frequency. The mercury prism cell was run with a side-arm temperature of 170 °C. A 300 μm slit was back-illuminated by diffuse laser scattering, and the light passing through the slit was collimated through the prism cell with an $f/10$ lens and then re-imaged at 0.895 m on to the microchannel plate of an intensified camera. The laser was tuned, and the wavenumber was monitored by a Burleigh wavemeter ($\pm 0.3 \text{ cm}^{-1}$). The measured displacement as a function of laser wavenumber is shown in Fig. 6 and compared with a Voigt model for the same geometry. The fit is best at a temperature of 168 °C, although the fit at 170 °C is within the data error bars.

The rotational Raman spectrum is recorded by tuning the laser to the center of the mercury vapor absorption manifold. For most molecules of interest, the rotational Raman lines are shifted by more than 10 GHz and fall out of the absorption band of the mercury. They are, however, very close to that band and fall within the highly refractive portion of the refractive index curve. The lines which fall at lower frequency than the mercury absorption lines encounter an index which is >1 and the light is

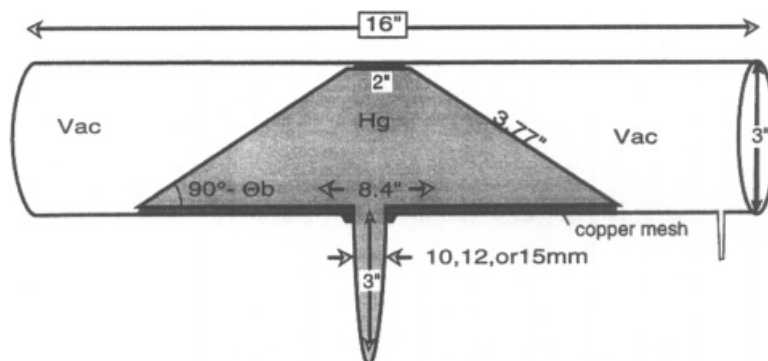


Figure 5. Schematic diagram of the Hg vapor prism. Concentric quartz cylinders allow for heating of the inner Brewster cut windows, while keeping the outer flat windows cool.

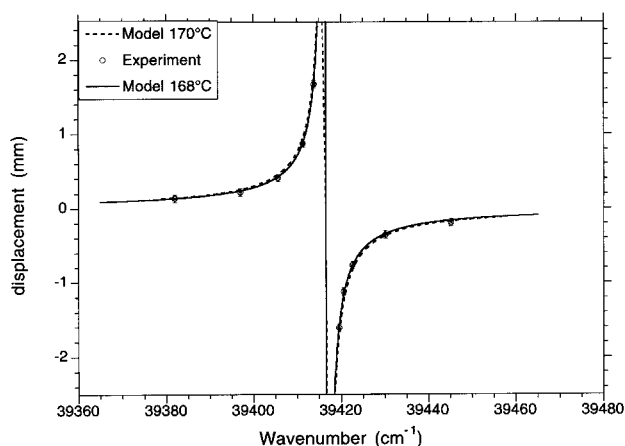


Figure 6. Vapor prism: measured and predicted deviation as a function of incident wavenumber.

refracted down. Those lines which fall above the mercury absorption encounter a refractive index <1 , and they are refracted up. The magnitude of the refraction increases as the frequency of the scattering approaches the mercury resonance. Those lines which are shifted from the laser frequency by the least amount are associated with transitions between the lowest lying rotational levels, and they are the most dispersed. Lines associated with higher lying rotational states are less dispersed, until light scattered far from the laser frequency and, thus, far from the mercury vapor frequency is essentially undeflected. Usually this includes the vibrational Raman lines, which fall one to three orders of magnitude further away from the driving laser frequency. In the vicinity of the mercury resonance, where the lower rotational lines fall, the dispersion of this Raman spectrometer is much higher than that of grating spectrometers. This suggests that this filter will more easily be able to resolve lines from individual molecular species, which are most easily distinguished at low rotational levels. Shifts associated with heavier molecules are smaller, so more complex molecules such as hydrocarbons will have more dispersed spectra. Tuning the laser with respect to the resonance can also increase the dispersion of particular spectral regions.

In the proof-of-concept experiment, CO_2 was used because it has a rotational B coefficient which is five times smaller than nitrogen ($B = 0.39 \text{ cm}^{-1}$ compared with 2 cm^{-1} for N_2), so the rotational lines are much closer to the driving laser frequency. The rotational Raman scattering cross-section of CO_2 is also about 6.5 times larger than N_2 . A comparison of the model predictions for both CO_2 and N_2 is shown in Fig. 7. For these measurements, the vapor pressure of the mercury is increased until absorption of the lowest rotational states is observed, so the cell dispersion is as large as possible. That corresponds to a vapor pressure of 12 Torr. Note that the $J = 0$ and $J = 2$ lines of CO_2 are strongly deflected, but also have significant absorption. On-line center attenuation of the cell was predicted to exceed 10^4 per cm. The experiment was conducted with the laser tuned slightly off the center of the line (7.7 cm^{-1}) so that attenuated Rayleigh scattering could be simultaneously collected. Since the Rayleigh scattering was closest to the mercury vapor line center, it was the most deflected. Figure 8 shows the collected spectrum from pure CO_2 . The image shows the dispersion in the vertical direction and is resolved along the $100 \mu\text{m}$

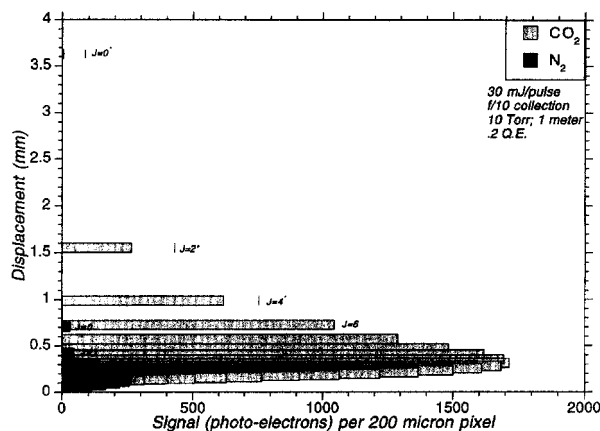


Figure 7. Model predictions for signal level and deviation of CO_2 and N_2 rotational Raman Lines. The asterisks indicate absorption of some fraction of incident radiation.

diameter laser line in the horizontal direction. The laser was operated at 30 mJ per pulse and the data in the figure represent a 50 shot average. The scattering was collected with an $f/5.8$ lens, collimated through the mercury cell, and imaged with a 0.895 m imaging lens on to a Princeton Instruments Pentamax CCD camera.

DENSITY GRADIENT RUBIDIUM CELL

The third approach again uses refractive index dispersion in the vicinity of an atomic resonance for Raman spectroscopy, but in this case the deflection arises from a density gradient across the cell rather than from refraction at the windows.⁷ The density gradient bends the light, just as light is bent in the thermally induced density gradient associated with a mirage. Therefore, by appropriate selection of filter length, the density gradient cell offers much stronger dispersion than its prism counterpart. It is important to note that for the rubidium cell, the maximum refractive index is limited by the temperature at which the rubidium reacts with the windows. In an atomic prism cell, contact with the windows is unavoidable, whereas in a gradient refractive index cell, windows can be removed from the atomic vapor, shielded by a buffer gas and cooled to temperatures far below the atomic vapor temperature. For this work, the main body of the cell was 10 in long, with a 5 in^2 cross-section. A reservoir at the bottom of the cell was filled with 10 g of high-purity (99.99%) rubidium. The cell was filled with a helium buffer gas at a pressure low enough to avoid thermally induced convective effects. As the bottom of the cell was heated, rubidium vapor diffused through the helium and condensed at the top, which was cooled. A narrow linewidth (1 GHz), tunable Ti : sapphire laser was used to measure the dispersion characteristics of the cell, which are shown plotted in Fig. 9, along with model predictions for bottom plate temperatures of 310, 292 and 212°C , and a constant top plate temperature of 60°C . A similar set of absorption curves for 287, 258 and 208°C with a constant 60°C top plate temperature are shown with model predictions in Fig. 10. The experimental configuration for the Raman measurement is shown in Fig. 11. The Ti : sapphire laser was tuned to overlap the center of the rubidium cell absorption, and the rotational Raman scattering from a CO_2 jet was collected through a slit, passed through the cell and imaged

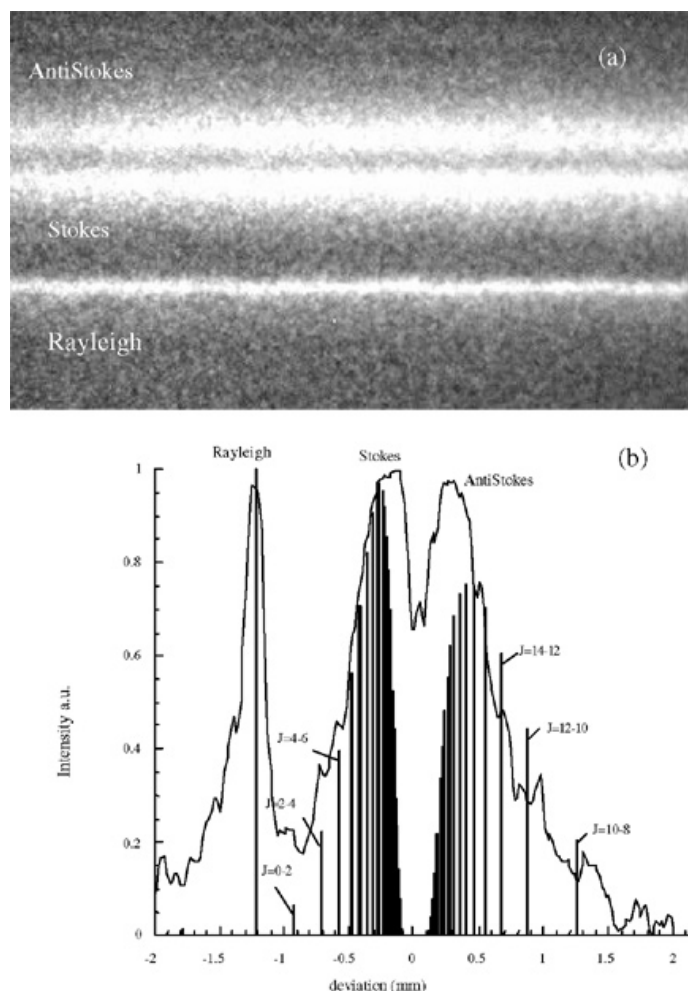


Figure 8. CO₂ rotational Raman scattering imaged with the mercury-vapor prism. (a) Raman scattering images of CO₂. (b) Intensity versus location for vertical cut through (a).

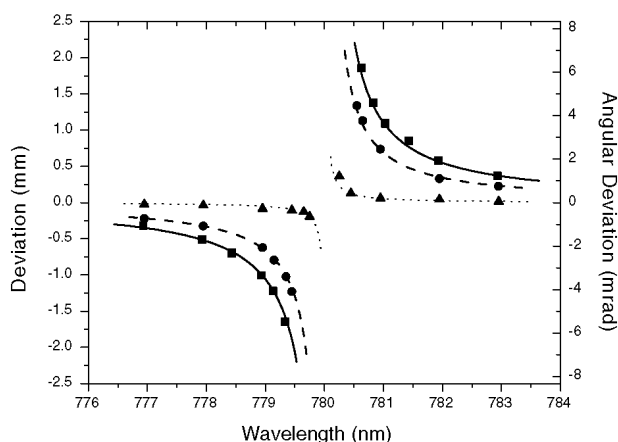


Figure 9. Measured and modeled deviation of light through the density gradient dispersive absorption filter as a function of incident wavelength. Measurements taken with (■) 310 to 60 °C, (●) 292 to 60 °C and (▲) 212 to 60 °C temperature gradients along with the modeled prediction. The right-hand vertical axis labels the angular deviation through the filter.

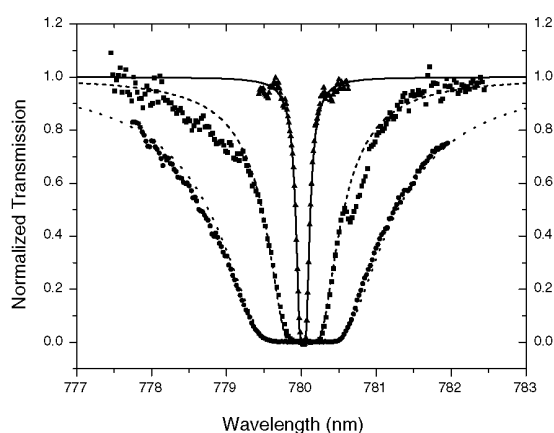


Figure 10. Measured and modeled predictions of the transmission profiles under various operating conditions. Data taken for temperature gradients of (●) 287 to 60 °C, (■) 258 to 60 °C and (▲) 208 to 60 °C. Also shown are the respective model predictions.

the absorption profile for the particular experimental conditions in this example.

CONCLUSION

The three examples presented in this paper indicate that the use of tunable lasers, together with atomic spectral

on to a second slit in front of a photomultiplier tube. The second slit was scanned in position, and the spectrum that was recorded is shown in Fig. 12. The locations of individual rotation lines are shown in the diagram. The lowest lying rotational states are not visible since they fall within

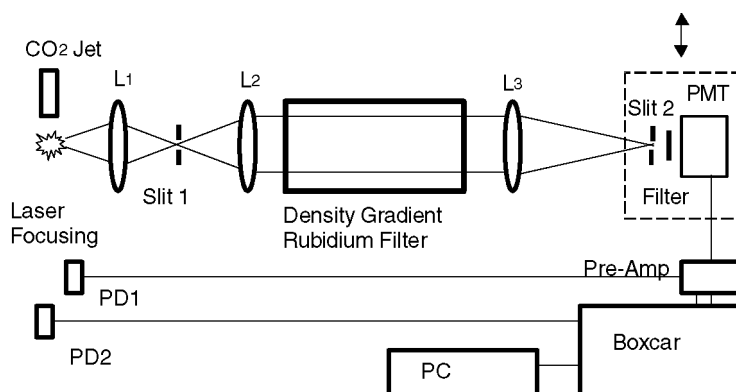


Figure 11. Schematic diagram for experimental setup. PD1 and PD2, photodiodes 1 and 2; L1, focal length 50 mm lens; L2, focal lens 250 mm lens; L3, focal length 300 mm lens. The interference filter used in this experiment was a 10 nm bandwidth passband filter.

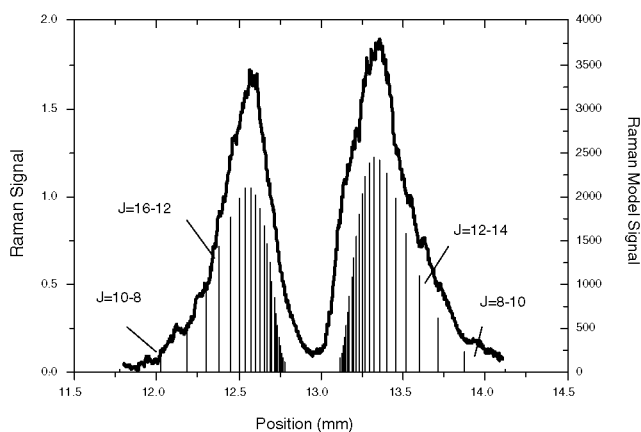


Figure 12. The 1-D carbon dioxide rotational Raman spectroscopic profile taken through the density gradient rubidium cell. Also shown are the numerical model predictions of the positions of each individual rotational line and its strength. The first few rotational Raman scattering lines are attenuated.

filters, is an attractive new way to perform rotational Raman spectroscopy. The refluorescence cell provides the capability of generating two-dimensional images of single Raman line scattering which may be useful for species

identification, species location and temperature measurements in fluid dynamic and combustion environments. With time gating and GHz-resolution spectral selectivity, the refluorescence filter strongly suppresses background noise. The refluorescence process, however, does contribute to additional signal loss, particularly for imaging applications. The dispersive filters have significantly higher efficiency and can be used to image the entire rotational Raman spectrum along a line. Two versions of these filters have been explored, a vapor prism and a gradient dispersion cell. The vapor prism has the advantage of simplicity and is demonstrated in the UV region using mercury vapor at 253.7 nm. The dispersive filter requires a density gradient and, therefore, introduces additional complexity, but has higher dispersive powers than the prism. This approach was demonstrated using rubidium vapor near 780 nm in the near-infrared region. For both dispersive cells, rotational Raman spectra from gas-phase CO₂ at atmospheric pressure were observed.

Acknowledgements

This work was supported by the Air Force Office of Scientific Research through the New World Vistas Program, the Air Plasma Ramparts MURI, and through a Small Business Innovative Research program with M. L. Energia, Inc.

REFERENCES

- Long MB, Fourquette DC, Escoda MC. *Opt. Lett.* 1983; **8**: 244.
- Nandula SP, Brown TM, Pitz RW. *Combust. Flame* 1994; **99**: 775.
- Brockhinke A, KohseHoinghaus K, Andresen P. *Opt. Lett.* 1996; **21**: 2029.
- Rothe EW, Andresen P. *Appl. Opt.* 1997; **36**: 3971.
- Finkelstein ND, Lempert WR, Miles RB. *Opt. Lett.* 1997; **22**: 537.
- Finkelstein ND, Yalin AP, Lempert WR, Miles RB. *Opt. Lett.* 1998; **23**: 1615.
- Miles RB, Lempert WR. *Annu. Rev. Fluid Mech.* 1997; **29**: 285.
- Forkey JN, Lempert WR, Miles RB. *Exp. Fluids* 1998; **24**: 151.
- Shay TM, Chung YC. *Opt. Lett.* 1988; **13**: 443.
- Gelbwachs JA. *IEEE J. Quantum Electron.* 1988; **14**: 1266.
- Gelbwachs JA, Chan YC. *IEEE J. Quantum Electron.* 1992; **28**: 2577.
- Menders J, Searcy P, Roff K, Korevaar E. *Opt. Lett.* 1992; **17**: 1388.
- Langberg E, Naylor M, Heckscher H. *Proceedings of Conference on Optical Instruments and Techniques*, Habell KJ (ed). Chapman and Hall: London, 1962; 229–237.
- Rabl A, Goodman NB, Winston R. *Solar Energy* 1979; **22**: 373.